Review on applications of X-ray computed tomography for coal characterization: recent progress and perspectives

Dameng Liu[a, b]*, Zheng Zhao[a, b], Yidong Cai[a, b], Fengrui Sun[a, b], Yingfang Zhou[c]

[a]*School of Energy Resources, China University of Geosciences, Beijing 100083, China*

[b]*Coal Reservoir Laboratory of National Engineering Research Center of CBM Development & Utilization, China University of Geosciences, Beijing 100083, China*

[c]*School of Engineering, Fraser Noble Building, King's College, University of Aberdeen, AB24 3UE Aberdeen, UK*

**Corresponding author. dmliu@cugb.edu.cn*

Abstract: Characterization of microscopic structure and macroscopic physical property are the basis for better understanding of coalbed methane reservoirs. X-ray computed tomography (CT), as an nondestructive measurement, has been widely and successfully applied to characterize the internal structure of coal. In this study, we introduce the principle of CT imaging and the microstructure recognition. A summary of CT imaging-based coal microstructure characterization follows, including three-dimensional (3D) microstructure reconstruction, pore and mineral quantification, and equivalent pore network model construction. We reviewed the methods used for evaluating the macroscopic properties of coal, including porosity calculation, gas adsorption/diffusion rate test, permeability simulation, and mechanical behavior evaluation. This study discusses the application of CT to investigate the evolutionary mechanisms of microstructure and macroscopic properties during gas adsorption, temperature change, and damage deformation. We conclude this review with a summary of the challenges and application perspectives of CT. The small scanning range, limited observation accuracy, functional limitations, lengthy testing process, and high cost are some of the major hurdles in the broad application of CT for coal characterization. In the future, CT should be combined with other techniques to establish full-scale pore and fracture models, identify mineral types in microstructures, and effusively use the advantages of CT by selecting the key points in the evolutionary

mechanisms of microstructure and macroscopic properties.

Keywords: Computation Tomography (CT); Coal Characterization; Microstructure; Macroscopic properties; Evolutionary mechanisms

1. Introduction

A comprehensive understanding of coal characteristics—such as adsorption, porosity, permeability, wettability, matrix deformation, and mechanical behavior,—is essential to design the exploration and development of coal and its associated gases.[1-3] The microstructure is the primary factor affecting the macroscopic properties of coal, and scholars have been studying it extensively using mercury intrusion porosimetry (MIP), liquid nitrogen adsorption, scanning electron microscopy (SEM), atomic force microscopy (AFM), and nuclear magnetic resonance (NMR).[4-6] MIP can be used to evaluate the porosity and pore-size distribution in coal; however, high pressures damage the pores,[7] and the samples cannot be recovered after the test. Liquid nitrogen adsorption can be used to investigate the pore-size distribution of coal when the pore-size range is limited to under 300 nm.[8,9] NMR cannot be used to ascertain the pore and fracture morphology when conducting quantitative microstructure characterization of the pores and fractures in coal.[10] However, SEM and AFM can be used to characterize the surface microstructures and morphology of pores and fractures,[11-13] but they are slightly inadequate for three-dimensional (3D) structure characterization. Compared to the aforementioned these techniques, X-ray computed tomography (CT) enables a visual description of the morphological characteristics of pores, fractures, and minerals in coal,[14,15] and the reconstruction of the 3D structure of coal.[16,17]

Studying coal characteristics using CT dates back to 1879, when scholars first used it to distinguish the organic and inorganic materials in coal.[18] At present, in addition to the microstructural characterization of coal, CT is widely used for investigating gas

adsorption, gas diffusion, permeability, mechanical behavior, and the evaluation of matrix deformation.[19-22] Previous reviews on CT application in coal characterization focused on pore and fracture characterization methods and 3D model establishment.[23,24] The influence of coal microstructures on macroscopic properties has been investigated by extensively studying the correlation between them, but the characterization of coal properties using CT has not been systematically reviewed yet.

Therefore, this study aims to extensively review the research on coal characterization conducted using CT. Furthermore, the imaging principle of CT and the recognition method of microstructure are introduced, and the research progress of CT in the quantitative characterization of coal microstructures and the qualitative evaluation of macroscopic properties is summarized systematically. The dynamics of microstructure and macroscopic properties under gas adsorption, temperature change, and damage deformation are discussed (Table 1). Finally, the challenges and application perspectives are considered, based on the limitations and advantages of existing studies on CT. This review lays the foundation for the in-depth application and development of CT in coal characterization.

Table 1 Research objectives and methods for CT in different applications

Applications	Research objects	Research methods
Microstructure	3D reconstruction	Work with 2D CT images.
	Pores and fractures	Calculate the content and fractal dimension of different scale pores and fractures based on a 3D reconstruction model of coal.
	Minerals	Calculate the content and fractal dimension of different scale minerals based on a 3D reconstruction model of coal.
Macroscopic properties	Porosity	Calculate using Avizo.
	Adsorption/diffusion	Perform CT tests based on the temperature increment method.
	Permeability	Establish a mathematical model or perform flow simulation.
	Mechanical behavior	Compare the mechanical behavior differences of coal samples with different microstructures.
Evolutionary mechanisms	Gas adsorption Temperature change Stress loading	Perform CT tests on the key points of coal matrix deformation and analyze the evolution of pores and fractures, porosity, and permeability of coal.

2. CT imaging and microstructure recognition

2.1 The principle of CT imaging

CT is a unique nondestructive testing technique that allows coal internal structure visualization, which is not achievable with conventional imaging techniques.[25-27] The basic principle of imaging is that after passing through the coal sample, the X-rays emitted by a ray source will be received by a detector, which converts the collected X-ray signal into a digital high-resolution image reflecting the information about the material components (Fig. 1(a)). When X-rays are emitted from the source and passed through materials of different densities, the light intensity is attenuated to different degrees due to reflection, scattering and refraction. The relation between light intensity and attenuation coefficient can be expressed as:[28,29]

$$I = I_0 e^{-\mu d} \quad (1)$$

where I_0 is the intensity of the incident X-ray, I is the intensity of X-ray received by the detector, μ is the attenuation coefficient when the ray passes through the object, and d is the thickness of the object.

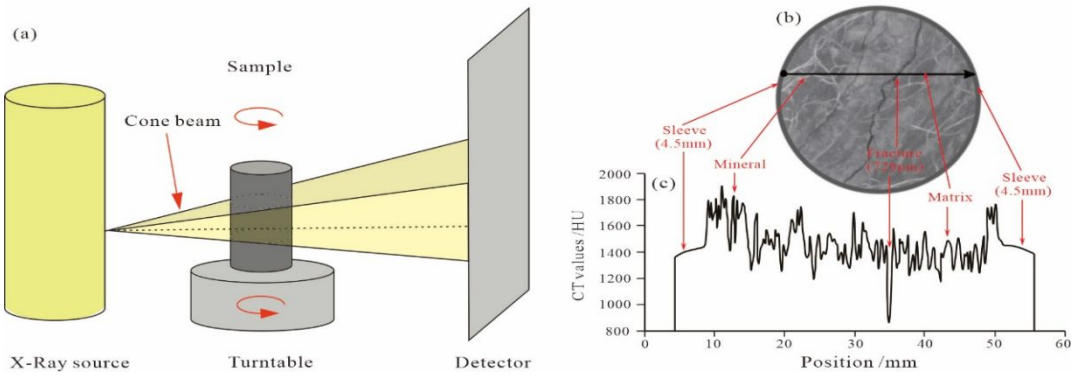

Fig. 1 (a) Schematic diagram of CT imaging principle. Modified with permission from ref 30. Copyright 2018 Elsevier B.V. (b) CT image. (c) CT values at different position. Fig. 1(b) and Fig. 1(c) are modified with permission from ref 32. Copyright 2014 Elsevier B.V.

After applying X-rays to the sample in a 360° full-angle step scan, the intensity values

of X-ray transmitted through the sample are monitored and recorded by a detector to obtain digital distribution information of the transmitted light intensity distribution at different angles. The X-ray attenuation coefficient distribution maps of each individual element of the sample can be obtained by converting and arranging the acquired signals, and then the CT images of different layers in the sample can be established.[24,30]

2.2 Recognition method of microstructure

Coal is composed of pores and fractures, minerals, and organic macerals (matrix). The minerals and matrix are the solid skeleton, and the pores and fractures are distributed within the skeleton.[31] Due to the differences in the density of pores and fractures, minerals, and matrix in coal, the attenuation coefficients of X-rays passing through different components also differs. The attenuation coefficient is linearly related to the density, which can be expressed as:[29]

$$\mu = \beta\rho \qquad (2)$$

where ρ is the sample density, and β is the Compton scatter constant of proportionality. Based on the Equations (1) and (2), different components in coal show different CT values in the images (see Fig. 1(c)). Therefore, the different components can be classified qualitatively according to the magnitude of CT gray scale values,[32,33] where the least dense of pores and fractures are shown as dark black, the high-brightness areas (white parts) are minerals, and the medium-gray areas are various organic macerals (matrix) (see Fig. 1(b)).

3. Quantitative characterization of microstructure

3.1 3D reconstruction of microstructure

In 2D CT slide, pores and fractures, minerals, and matrix of coal sample can be easily identified, allowing a qualitative characterization of the microstructure in a certain

cross-section. However, 3D reconstruction using CT images is required for characterization and analysis of the overall microstructure inside the coal sample.

In the 3D reconstruction of the coal microstructure, the specific grayscale ranges of pore fractures, minerals, and matrix normally determined by threshold segmentation.[34,35] As an important basis for 3D reconstruction, the accuracy of threshold determines the accuracy of the final 3D reconstruction model,[36] and the existence of noise in the image makes it inevitably deviate from the real image.[37] Therefore, the CT images usually requires further processed, including adjusting the image contrast, filtering the scatter dots noise, priors to segmentation.[38-41] Use the pre-processed 3D image, the threshold segmentation is calibrated along with measured porosity (MIP or other methods), and then to obtain the 3D coal microstructure (see Fig. 2).[34,42,43]

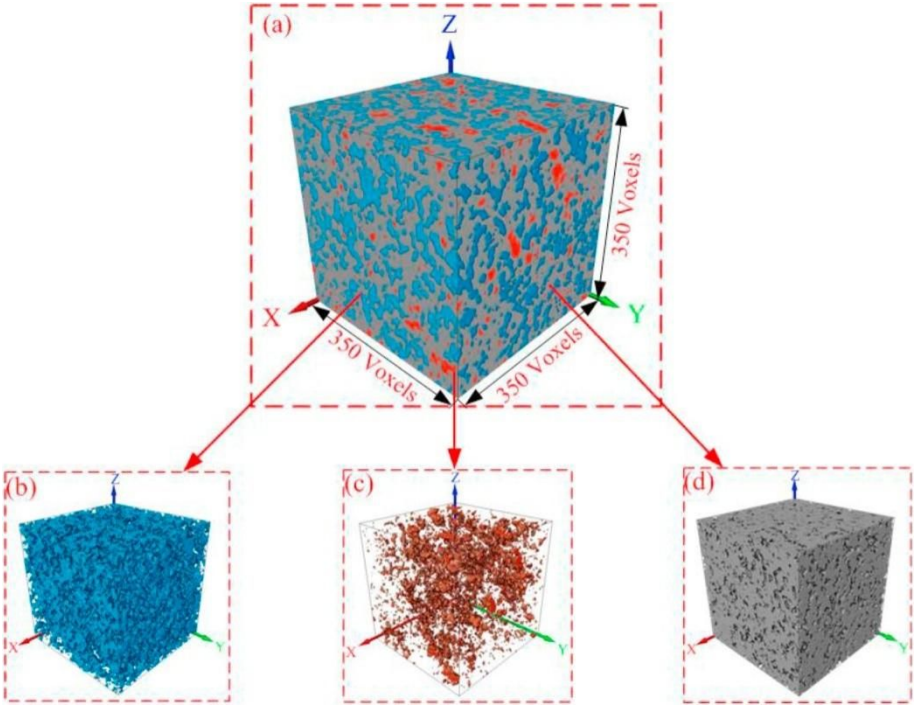

Fig. 2 3D reconstruction model of coal microstructure. (a) 3D reconstruction model of the whole coal rock; (b) pore and fracture model; (c) mineral model; (d) organic maceral model. Reproduced with permission from ref 43. Copyright 2020 Elsevier B.V.

3.2 Characteristic of pores and fractures

Coal is a dual-pore structure rock, with internal pores and fractures serving as storage space and flow channels for coalbed methane, respectively.[44,45] Quantitative characterization of the microscopic parameters of pores and fractures in coal are essential for coal porosity and permeability evaluation.[46]

3.2.1 Distribution of pores and fractures

The pore size, scale of fractures, and pore and fracture locations are vital microscopic parameters of coal. Pores and fractures are formed in the entire process of coal rock sedimentation and evolution, and the differences between the formation conditions of different periods and types of pores and fractures increase the complexities in their forms and sizes.

When characterizing the distribution of pores with varying coal sizes, it is standard to consider each pore as a sphere equal to its volume and calculate its equivalent size.[22] The calculation formula can be expressed as:

$$D_{eq} = \sqrt[3]{6V_{pore}/\pi} \quad (3)$$

Where D_{eq} is the equivalent pore size (μm), and V_{pore} is the individual pore volume (μm^3).

When describing the distribution characteristics of fractures with different scales in coal, the types were firstly classified based on the width of fractures (W) and the length of fractures (L), where type A: W > 5 μm and L > 10 mm; type B: W > 5 μm and 1 mm ≤ 10 mm; type C: W < 5 μm and 300 μm < L < 1 mm; and type D: W < 5 μm and L < 300 μm.[47]

In the 3D pore and fracture model (Fig. 2(b)), the distribution of pores and fractures in coal can be quantitatively characterized by separately labeling the pores of varied sizes and fractures of different scales using the Avizo software (Fig. 3).[48-50]

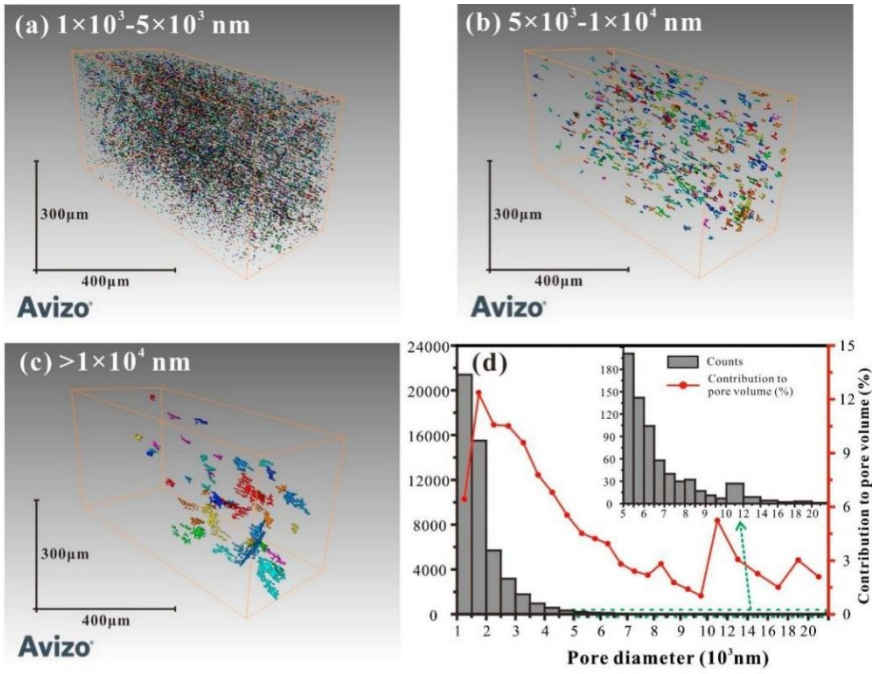

Fig. 3 Distribution characteristics of pores and fractures with different sizes. (a) 1×10^3-5×10^3 nm. (b) 5×10^3-1×10^4 nm. (c) more than 5×10^3 nm. (d) The counts and contribution of pores and fractures with different sizes. Reproduced with permission from ref 49. Copyright 2017 Elsevier Ltd.

3.2.2 Fractal characteristics of pores and fractures

Fractal dimension is an important parameter reflecting the complexity and irregularity of fractal objects.[20,51] Among many fractal methods, the box counting method is widely used in the characterization of pore and fracture fractal features in coal due to its simplicity and computability.[52-54]

When using this method to calculate the fractal dimension of pores and fractures in 2D images obtained from CT, a square study range should first be determined and the pores and fractures within the range should be extracted. Then it is covered using a square grid of equal size to the study range with the edge lengths uniformly divided into *r* equal parts,[55] and the number of non-spaces *N*r among them is counted. The number of non-spaces has a certain correlation with the grid edge lengths and the 2D fractal dimension.[56]

$$N_r \sim r^{-D} \quad (4)$$

The 2D fractal dimension D_2 can be obtained from the slope of the fitted curve of Nr versus r.[57]

$$D_2 = -\lim_{r \to 0} \frac{lg\, N_r}{lg\,(r)} \quad (5)$$

In the same manner, the volume fractal dimension of the 3D pore and fracture structure can be calculated. After determining the study area and extracting the 3D pore and fracture structure, it is covered with square boxes of equal size to the study area with the side lengths uniformly divided into ε equal parts, and the number of non-empty boxes $N\varepsilon$ among them is counted, then the volume fractal dimension D_3 can be expressed as:[15]

$$D_3 = -\lim_{\varepsilon \to 0} \frac{lg\, N_\varepsilon}{lg\,(\varepsilon)} \quad (6)$$

Counting Nr (or $N\varepsilon$) at different values of r (or ε) using the above method and plotting a scatter plot of the logarithm of Nr (or $N\varepsilon$) versus the logarithm of r (or ε). Then its slope, which is the fractal dimension D_2 (or D_3), can be obtained using the least squares method.

3.2.3 Equivalent pore network model

The 3D reconstructed pore and fracture model (Fig. 4(a)) of coal sample can reflect the morphological characteristics and spatial distribution of pores and fractures inside the sample. However, the complex pore and fracture structure makes the application of this model for fluid seepage and other simulations very computationally intensive. In order to optimize the calculation process, a simplified equivalent pore network model with topological structure was developed.[58,59]

The equivalent pore network model effectively includes the geometric features of pores and fractures in coal (Fig. 4(b)). Its establishment not only solves the problem of

excessive computation during the simulation, but also enables the statistics of parameters such as throat length and coordination number, which are important for studying the connectivity of coal. The pore space and pore throat can be extracted separately in this model, which can describe the distribution of pore space and pore throat more clearly.[60] Meanwhile, the maximum sphere algorithm is used to calculate the coordination number of pore network and the pore throat distribution of coal sample,[61,62] which is the fundamental for coal permeability calculation.

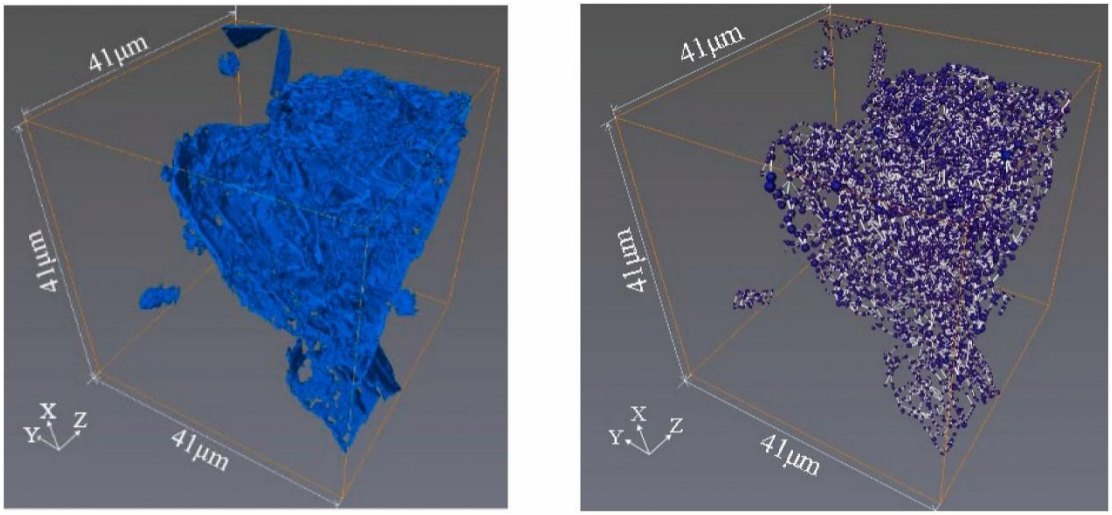

(a) (b)

Fig. 4 3D visualization of microfractures. (a) Reconstructed microfracture network. (b) Pore network model skeleton of the microfractures. Reproduced with permission from ref 59. Copyright 2020 Elsevier B.V.

3.3 Characteristic of minerals

Minerals, which have a relatively high density, are one of the components that make up the coal skeleton. The characteristics such as content, size, distribution, and complexity of minerals have important effects on the flow of fluids in the coal and the mechanical behaviors of the coal. Based on the 3D mineral model of coal (Fig. 2(c)), the mineral characteristics in coal can be evaluated quantitatively.[63,64]

The equivalent diameter is an important parameter for quantifying the irregular

structure.[65] Similar to analysis of pores and fractures, minerals can be divided into four categories according to their equivalent diameters: small-size minerals with an equivalent diameter $d \leq 500$ μm, medium-size minerals with 500 μm $< d \leq 1000$ μm, larger-size minerals with 1000 μm $< d \leq 2000$ μm and large-size minerals with $d > 2000$ μm. According to Eq. (3), the equivalent diameter of minerals can be calculated. Then, the content and volume of minerals at different scales can be counted using Fig. 2(c). Based on this, the fractal dimension of minerals can be calculated according to Eq. (6), and then the complexity of mineral structure can be evaluated.

4. Qualitative evaluation of macroscopic properties

The microstructure of coal is the fundamental factor affecting its macroscopic properties. In addition to be simulated and tested directly, the macroscopic properties of coal can be quantified by establishing the relationship between different microstructural parameters and macroscopic properties.

4.1 Porosity

Porosity refers to the ratio of the total volume of pores and fractures in the coal sample, including unconnected and dead pores that are closed, to the volume of the study area, and this parameter directly reflects the development degree of pores and fractures in coal. However, interconnected pores and fractures in coal are the actual spaces and channels for fluid storage and flow, and the effective porosity calculated from the volume of interconnected pores and fractures is a better guide for evaluating the adsorption, diffusion, and seepage properties of coal. By using the Avizo software, the volumes of interconnected pores and fractures in the 3D pore and fracture model are determined, and the effective porosity of the coal samples can be calculated.[66] The equation can be expressed as:[67]

$$\varphi = \frac{V_{pc}}{V} \times 100\% \quad (7)$$

where φ is the effective porosity of the coal sample (%), V_{pc} is the volume of interconnected pores and fractures (μm^3), V is the total volume of the studied part of the coal sample (μm^3).

According to Eq. (7), by extracting pores and fractures at different scales from the 3D pore and fracture model, the porosity of pores and fractures at each scale and their contribution to the effective porosity can be calculated separately. The pore and fracture volumes and porosity of the coal samples correlate with the size of the constructed model,[68] and after comparing the pore and fracture characteristics of the constructed models with different sizes of coal samples, it was found that the larger the model size, the larger is the porosity of the study area.[40]

4.2 Adsorption and diffusion

Coal is a natural porous medium, and the complex combination of pores and fractures affects the adsorption, diffusion, and seepage patterns of gases in coal.[69] Among the full-scale pores and fractures in coal, pores smaller than 100 nm constitute a relatively small proportion of the total pores, but they contribute to a majority of the specific surface area (Fig. 5). This scale of pores, which significantly influences the adsorption capacity and kinetic characteristics of coal, is the main space for gas adsorption in coal, and pores smaller than 100 nm are typically defined as adsorption pores.[70,71]

The density variation and temperature increment methods are used to evaluate the gas content in coal using CT. The free gas content test based on the density variation of coal samples is primarily performed for inert gases.[72,73] This method first determines the density distribution of coal based on the CT images of vacuum coal samples. Subsequently, a CT test is performed on the coal samples after the gas invasion. In the test results after inert gas filling, both the matrix and gas in pores and fractures cause

X-ray attenuation, and the X-ray attenuation coefficient caused by the gas at each location can be expressed as follows:

$$\mu_k = \mu - \mu_c \quad (8)$$

where μ, μ_c and μ_k are the attenuation coefficient when the X-ray passes through the vacuum coal sample, gas filling coal sample, and gas respectively.

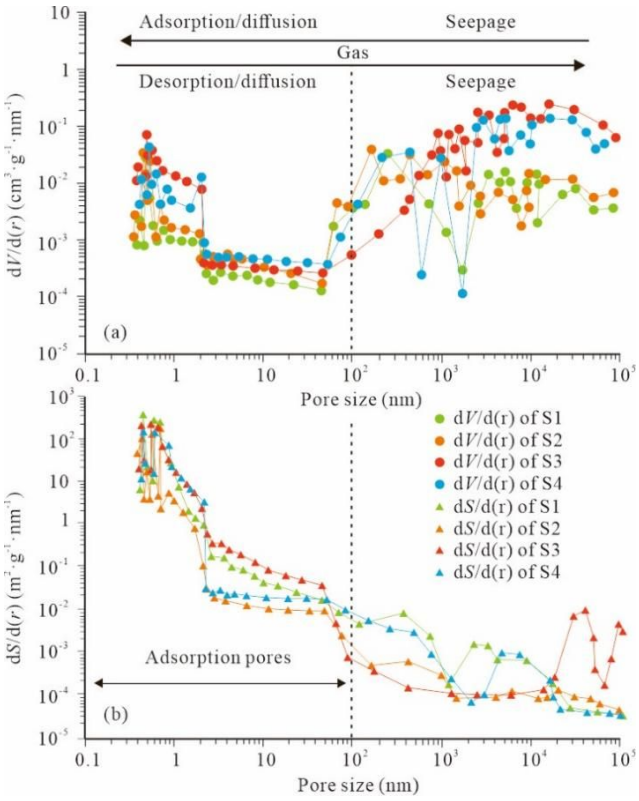

Fig. 5 (a) Volumes and (b) specific surface areas distribution of pores with different sizes in coal. Modified with permission from ref 71. Copyright 2019 Elsevier B.V.

The gas density in coal pores and fractures can be obtained using equations (2) and (8). The free gas content in coal can be calculated based on the pore and fracture volumes. The degree of development of effective pores and fractures in coal primarily influences the free gas content; the larger the effective porosity of coal, the larger is the space for gas storage and the greater is the amount of free gas.

For gases primarily adsorbed in coal, such as CO_2 and CH_4, the gas content testing

method based on the density variation is inapplicable owing to the matrix expansion occurring when coal adsorbs these gases. The primary approach for CT-based gas adsorption measurement in coal is the temperature increment method, which considers that the increase in the system's temperature is proportional to the gas adsorption amount. The gas adsorption rate and amount can be calculated based on the system temperature change during the experiment and the final temperature increase in the system after the adsorption equilibrium.[74,75]

After CO_2 and CH_4 enter the coal through the fracture network, they transfer between the fractures and coal matrix via diffusion. The gas adsorption rate in coal primarily depends on the gas diffusion rate; therefore, the diffusion rate is evaluated based on the gas adsorption rate. The adsorption kinetic characteristics of coal samples at various pressures and in various regions are evaluated using the temperature increment method, and Fig. 6 shows the variation curves of the increment in system's temperature with time.

As shown in Fig. 6(a), the coal adsorption amount increases with the increase in gas pressure, and the gas adsorption/diffusion rate also increases. The pressure/concentration difference affects the coal's gas adsorption/diffusion rate. The gas adsorption/diffusion rate is more significant at the beginning of adsorption when the pressure/concentration difference is larger. As the pressure/concentration difference gradually decreases, the adsorption/diffusion rate gradually decreases and finally reaches adsorption equilibrium. The gas adsorption/diffusion process can be divided into fast increasing, slow increasing, and stable stages.

A comparison of the temperature increment variation curves for different microstructures of the coal samples showed that the overall gas adsorption is low, and the gas adsorption/diffusion rate in regions with fewer pores and fractures (A1, A2, and

A3) is lower than in regions with well-developed pores and fractures (B1, B2, and B3) (Fig. 6(b) and Fig. 6(c)). Similarly, the gas adsorption/diffusion rate in regions with more clay minerals (C1, C2, and C3) is lower than in the normal regions (B1, B2, and B3) (Fig. 6(c) and Fig. 6(d)). The gas adsorption amount and the adsorption/diffusion rate are positively correlated with the pore and fracture contents but negatively correlated with the mineral content.[74]

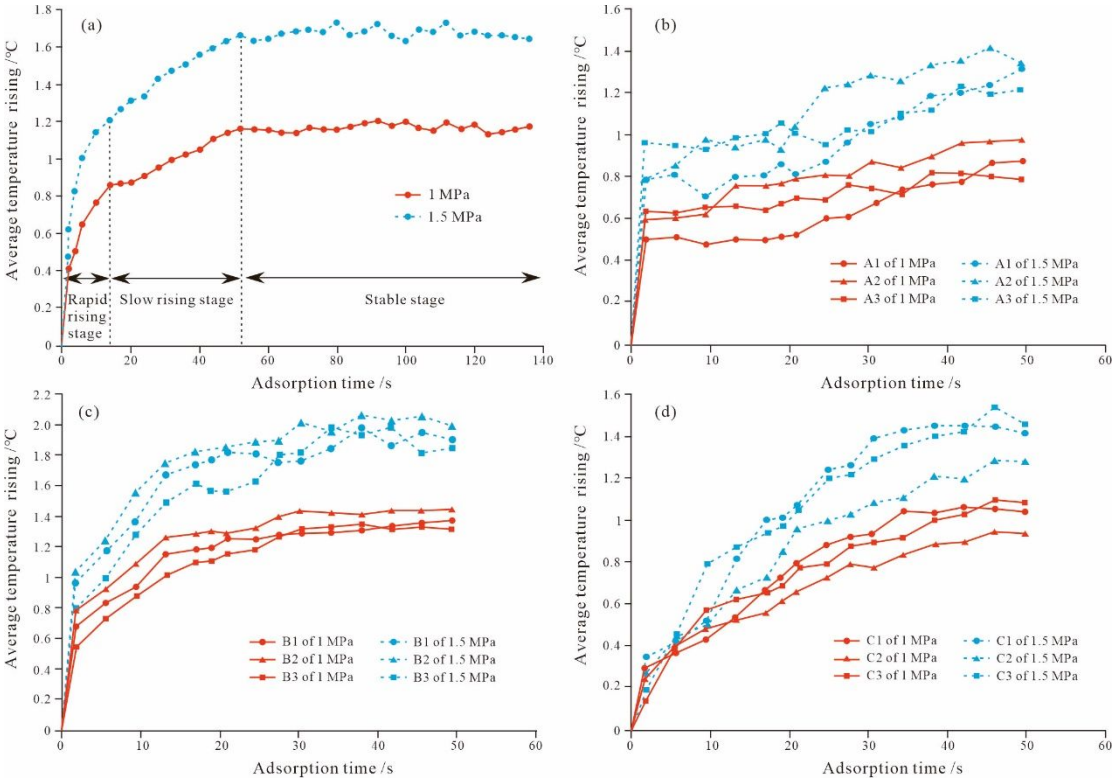

Fig. 6 Temperature rise characteristics of coal with CH_4 adsorption. (a) The overall trend. (b) Regions with fewer pores and fractures. (c) Regions with a well-developed pores and fractures. (d) Regions with more clay mineral. Modified with permission from ref 74. Copyright 2016 Elsevier B.V.

Furthermore, the different molecular properties of various gases lead to differences in their adsorption kinetic characteristics in coal. Since the molecular weight of CH_4 is lower than that of CO_2, the adsorption/diffusion rate of CH_4 is more significant than that of CO_2 at the low-pressure stage. However, the CO_2 adsorption affinity is higher than that of CH_4, and the CO_2 adsorption/diffusion rate increases and gradually exceeds

that of CH_4 as the pressure increases.[76] The difference in the coal's adsorption characteristics for different gases provides an essential theoretical basis for studying CO_2-enhanced coalbed methane recovery (CO_2-ECBM).[77,78]

4.3 Permeability

Permeability is a crucial parameter in the physical properties of coal reservoirs, and there are two primary methods for evaluating the permeability using CT according to the influence of the type, development, distribution, scale, connectivity, and filling of pores and fractures in coal. On the one hand, a mathematical model of permeability evaluation can be established based on the quantitative characterization of the microstructures of coal.[5] On the other hand, a fluid flow simulation in coal can be performed using the Avizo software based on the equivalent pore network model of coal, and the permeability of coal can be evaluated.[79,80] Accordingly, the degree of influence of different parameters on permeability can also be evaluated by comparing the correlation between permeability and each pore and fracture parameter.

During seepage simulations, the differences in flow rates in different coal regions reveal that areas with developed pores and fractures, good connectivity, and large pore throat size exhibit high flow velocity zones. The pore throat radius decreases in the fluid's medium velocity region due to the poorly developed pores and fractures in the coal sample, resulting in a weak connectivity between the pore throat channels and a partial momentum loss when the fluid passes through the seepage channels. The connectivity of pores and fractures is poor in the coal sample's outer parts; consequently, the fluid's flow velocity is the lowest in these parts (Fig. 7).

Differences in the pore and fracture structures in coal at different flow rate regions reflect the microstructural influence on the macroscopic permeability of coal. The

seepage velocity of the fluid in coal correlates well with the degree of pore and fracture development, connectivity, and pore throat size.[81] The more developed the pores and fractures are, the better is their connectivity, and a larger pore throat size in coal leads to a higher flow rate and a better permeability.[82] The effect of these three factors on permeability is in the following order: pore and fracture connectivity > pore throat size > pore and fracture development.[83] To some extent, the coal's permeability tends to increase with the increase in effective porosity;[84-86] however, this trend is not absolute,[87] and effective porosity is not a single influence on permeability. Low porosity is a sufficient nonessential condition for low permeability, whereas high permeability is a sufficient nonessential condition for high porosity.[88-92] Furthermore, the fractal dimension value primarily reflects the roughness and complexity of pores and fractures in coal[14,21] and correlates with coal permeability. Coal samples with higher fractal dimensions usually have lower permeability,[57] and this relationship is pronounced in higher-order coals.

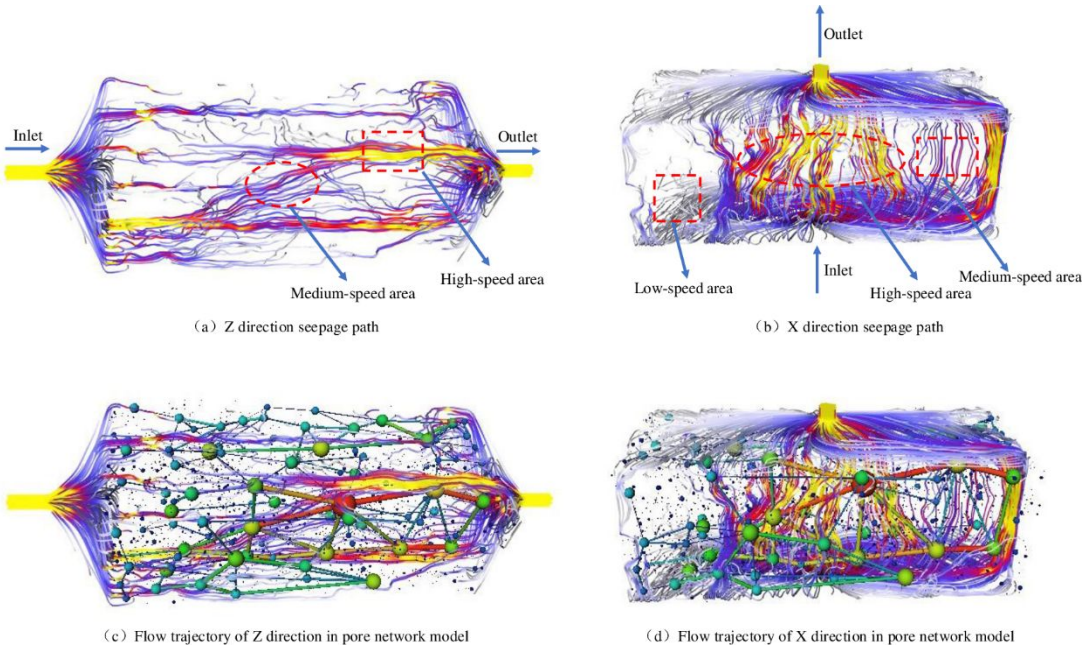

(a) Z direction seepage path (b) X direction seepage path

(c) Flow trajectory of Z direction in pore network model (d) Flow trajectory of X direction in pore network model

Fig. 7 Simulation results of the flow pattern of fluids in coal (the fluid direction is set to flow from left to right, and the gray flow lines represent the low velocity region of seepage; the purple flow lines

represent the medium velocity region of fluid; the yellow flow lines represent the high velocity region of fluid). (a) Z direction seepage path. (b) X direction seepage path. (c) Flow trajectory of Z direction in pore network model. (d) Flow trajectory of X direction in pore network model. Reproduced with permission from ref 83. Copyright 2021 Jing et al. Authors under Creative Commons Attribution 4.0 International License (CC BY 4.0).

4.4 Mechanical behavior

The complex microstructure makes coal highly heterogeneous, resulting in significant differences in gas adsorption, diffusion, and seepage patterns and causing substantial differences in the strength and compressibility of coal at different locations.[93,94] CT cannot be used to directly test and simulate the mechanical behavior of coal, but the effect of the microstructure on the mechanical behavior of coal can be obtained by comparing the mechanical behavior differences in coal samples with different microstructures.

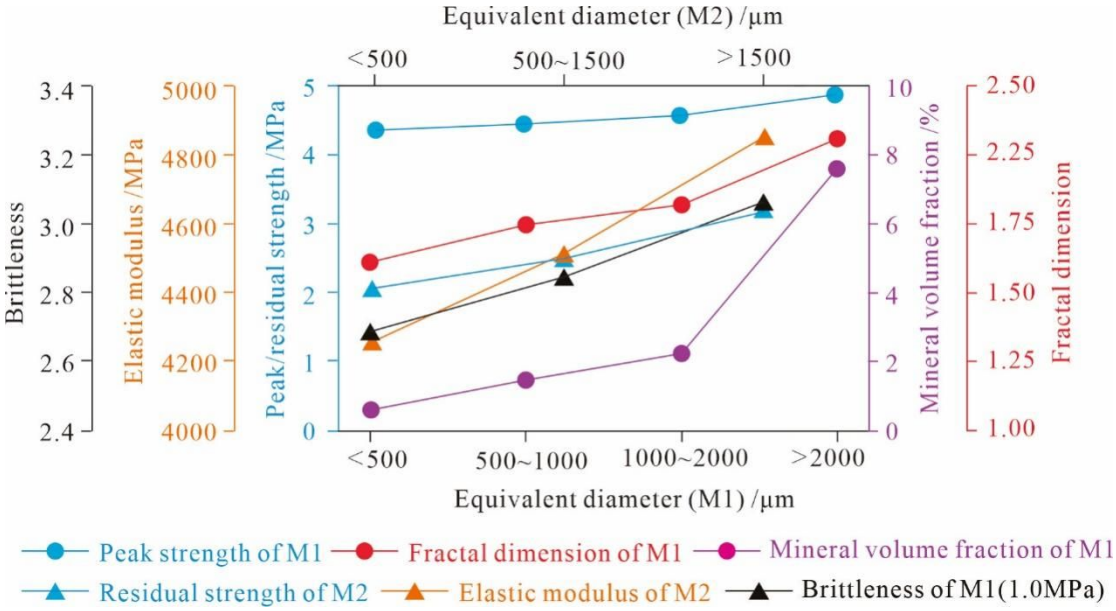

Fig. 8 Relationship between macroscopic mechanical behavior of coal and microscopic parameters of minerals. Modified with permission from refs 64, 65. Copyright (ref 64) 2020 The Authors, published by Journal of Mining & Safety Engineering. Copyright (65) 2020 Yu Fu and Zhongliang Feng. Authors under Creative Commons Attribution 4.0 International License (CC BY 4.0).

The geometry, size, and distribution of irregular minerals in coal are primary factors that constitute its heterogeneity characteristics and significantly influence the macroscopic mechanical behavior of coal. The specific influence of minerals on the mechanical behavior of coal has been investigated by constructing finite element models containing different mineral structures and performing uniaxial compression simulations.[64, 65] The results showed that the larger the size and higher the content of minerals, the more complex is the distribution. Under uniaxial conditions, the presence of minerals and the increase in mineral sizes increase the peak strength, elastic modulus, and residual strength of coal (Fig. 8). When a specific circumferential pressure is applied, the minerals reduce the coal's brittleness. The difference in density between the coal matrix and the minerals creates a discontinuity surface that allows the fractures generated during coal breakage to propagate along the junction of the minerals and the coal matrix.[95]

In addition to minerals, the degree of pore and fracture development,[96,97] distribution characteristics,[98] and connectivity of pores and fractures have a direct influence on the mechanical properties of coal.[99] Initial fractures are critical factors affecting the strength and failure patterns of coal samples.[21,100-103] On the one hand, the presence of pores and fractures weakens the ability of coal to store elastic strain energy and undergo impact damage. On the other hand, original pores and fractures affect the coal's fracture location, and most of the final fracture surface will pass through the initial fracture during coal damage. Overall, the larger the fracture size and higher the development of fractures in the coal, the lower is its compressive strength.[104,105] Coal strength is negatively correlated with the logarithm of porosity, and the elastic modulus decreases with increasing initial damage.[104]

5. Dynamic evolution of microstructure and macroscopic properties of

coal

The coal matrix is deformed due to gas adsorption, temperature change, and stress loading. For visualizing the dynamic evolution of coal microstructures during this complex deformation process, calculating and simulating the changes in macroscopic properties (e.g., porosity and permeability) are vital to understand the mechanisms of coal matrix deformation.

5.1 Gas adsorption

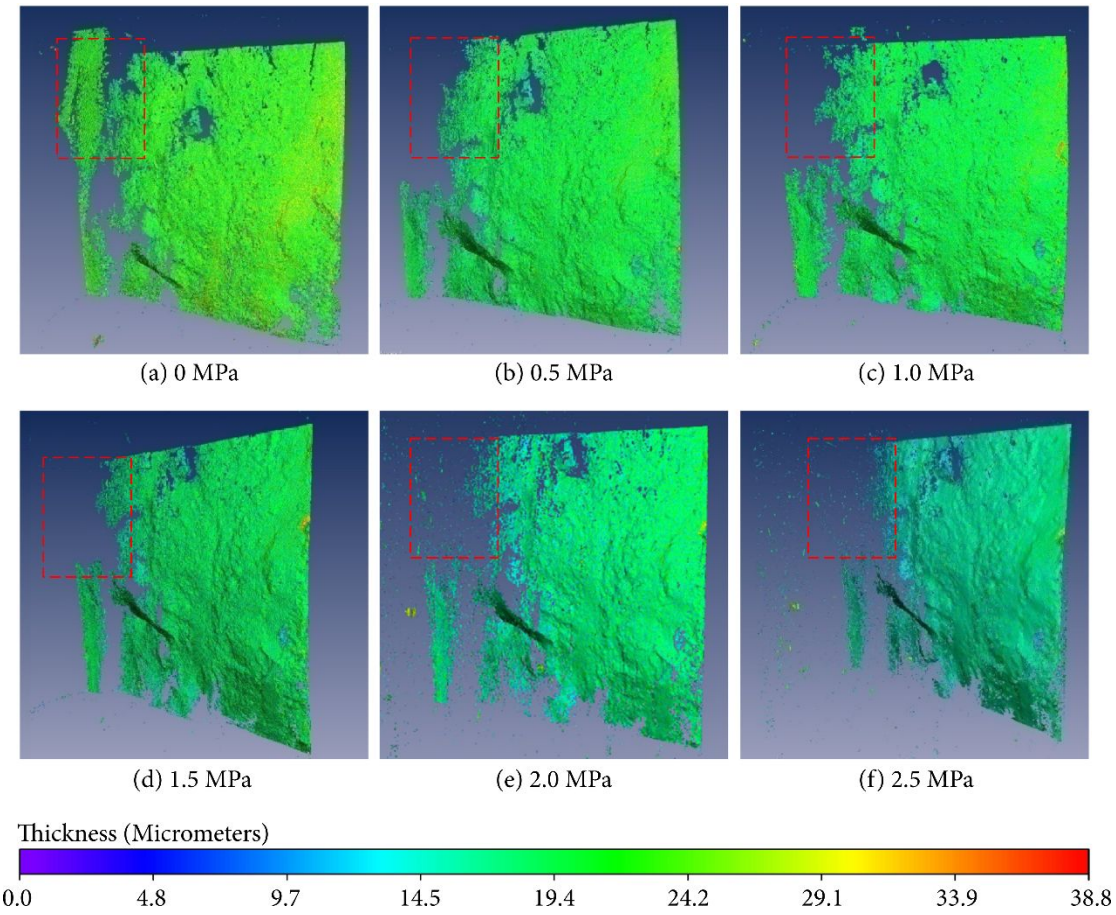

Fig. 9 Characteristics of fracture evolution under different pressure based on CT pseudocolor images. Reproduced with permission from ref 106. Copyright 2018 Xiangrong Nie et al. Authors under Creative Commons Attribution 4.0 International License (CC BY 4.0).

Coal is a natural heterogeneous porous medium with strong adsorption properties. The coal matrix will experience swelling deformation after the adsorption of gases, such as

CH_4 and CO_2, and the change in the internal microstructure will further cause changes in the macroscopic properties of coal. Deformation of the coal matrix during gas adsorption is a complex process. As gas adsorption requires the coal sample to continuously remain under the adsorption pressure, it is challenging to characterize the coal's microstructure during the adsorption process using conventional experimental instruments. The development of CT technology has solved this problem by evaluating the pore and fracture structures of coal under different adsorption conditions and analyzing the evolution of pore and fracture volume and porosity of coal during gas adsorption.

Adsorption time, adsorption pressure, and the microstructure affect the swelling deformation of the coal matrix after gas adsorption, and the changes in the porosity and permeability of coal after adsorption are closely related to the gas pressure in the pores and fractures and the degree of coal matrix swelling deformation. By evaluating the internal microstructure of coal under different adsorption pressures using CT and simulating coal swelling deformation using the Avizo software, the results showed that as the adsorption pressure of gas increases, the thickness of typical fractures in the coal decreases significantly, causing a negative exponential decrease in porosity and permeability.[106,107] The preswelling stage of the coal matrix shows a significant decrease in fracture length, followed by a substantial decrease in fracture width.[41]

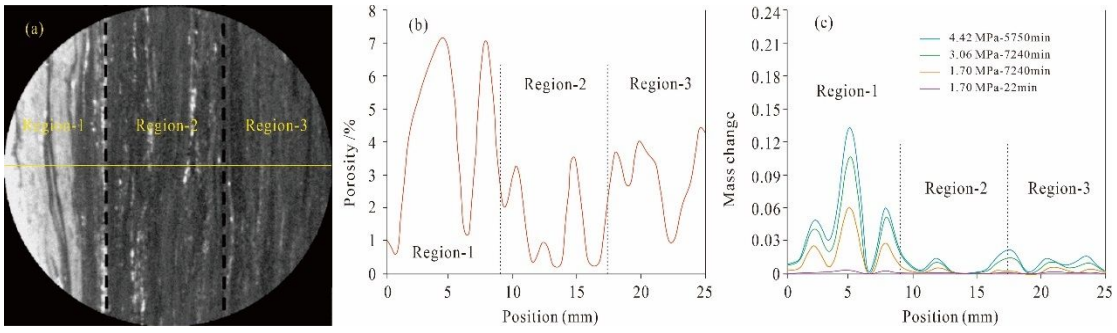

Fig. 10 The deformation difference of different areas in coal after adsorption of CO_2. (a) CT image of

coal (b) Porosity of coal at different positions. (c) Mass changes under different gas pressure and time at different regions. Modified with permission from ref 107. Copyright 2003 Elsevier Science B.V.

In addition to increasing the adsorption amount and enhancing the matrix swelling deformation, the gas pressure promotes the porosity and permeability of coal. For the loaded coal samples, the reduction in effective stress caused by the entry of high-pressure gas into the coal fractures immediately increases the fracture size. Then, the matrix swelling deformation becomes more robust with the continuous gas adsorption, and the fracture scale decreases.[108] When the matrix contraction caused by effective stress reduction and the matrix expansion caused by gas adsorption occur simultaneously, the low-density structure tends to shrink, the high-density structure tends to expand, and a local uniformity can develop in the coal density.[109,110]

Before the coal samples reach the adsorption equilibrium, the swelling deformation of coal increases continuously with the increase in adsorption time. However, the mass variation of coal varies significantly in different microstructure regions.[75,107,109] The regions with higher porosity, where the adsorbed gas amount is high, show a greater degree of overall mass change in the coal matrix after CO_2 adsorption, whereas the lower porosity areas have an overall lower degree of mass change after the adsorption (Fig. 10). Furthermore, the deformation during adsorption and desorption of the coal matrix is irreversible. Pores and fractures will only partially recover after gas desorption, and the coal matrix swelling deformation will gradually decrease when multiple gas adsorption–desorption cycles are performed.[111]

5.2 Thermal effect

The coal skeleton comprising minerals and organic macerals is highly temperature-sensitive, and its microstructure and macroscopic properties change significantly when

the coal's temperature changes. The internal microstructures and macroscopic properties of coal samples differ considerably before and after thermal shock, microwave heating, and liquid CO_2 freezing–thawing. The coal matrix generates numerous fractures as the temperature increases. The increase in the number and width of fractures and the volume of pores and fractures increase the coal's porosity and permeability, and this increase is positively related to the increase in heating time and the temperature of coal.[112-114] The coal's volume and matrix densities decrease after liquid CO_2 freezing–thawing, and the generation and transformation of numerous pores and fractures in coal significantly increase the coal's porosity.[115] To further study the pore and fracture evolution mechanisms during the change in temperature of coal, the pore and fracture changes in four coal samples from three ranks (low, medium, and high coal ranks) listed in Table 2 during the temperature change were evaluated. The obtained CT images and the plotted porosity evolution curves of the coal samples at different temperature stages are shown in Fig. 11.

Table 2 The basic characteristics of each coal sample studied

Coal sample ID	Coal rank	Coal types	Ash (%)	Moisture content (%)	Volatile mater (%)	Sulphur content (%)
R1-1 [116]	Low-rank	Lignite	21.00	1.86	39.80	1.43
R1-2 [117]	Low-rank	Lignite	-	-	-	-
R3 [118]	Medium-rank	Lean coal	28.01	0.84	35.73	0.51
R4 [119]	High-rank	Anthracite	12.47	1.24	8.95	1.44

As shown in Fig. 11, the coal samples' pore and fracture structures change significantly when the temperature increases, but the overall porosity is not positively correlated with temperature. The evolution of porosity with temperature varies in the coal samples of different coal ranks (Fig. 11(a)).

The porosity of the low-rank coal sample (R1) shows three primary stages of "rapid increase–smooth–rapid increase" with increasing temperature. As evident from the CT

images taken at different temperature stages, the temperature of the low-rank coal sample increases to 200°C, and the water and free gas dissipation ruptures the coal matrix. The scale of the original pores and fractures in the coal increase visibly, generating new pores and fractures, and the overall porosity increases significantly. When the temperature varies between 200°C and 400°C, the positive effect for the pores and fractures increases caused by the dissipation of water and free gas gradually weakens, and the negative effect for the reduction in pores and fractures caused by coal matrix expansion after the temperature change increases. Under the coupling of the above two effects, the overall porosity changes relatively smoothly. When the temperature exceeds 400°C, the low-rank coal sample pyrolyzes. As a result, the scale of pores and fractures increases, and the overall porosity grows further (Fig. 11(b)).[117]

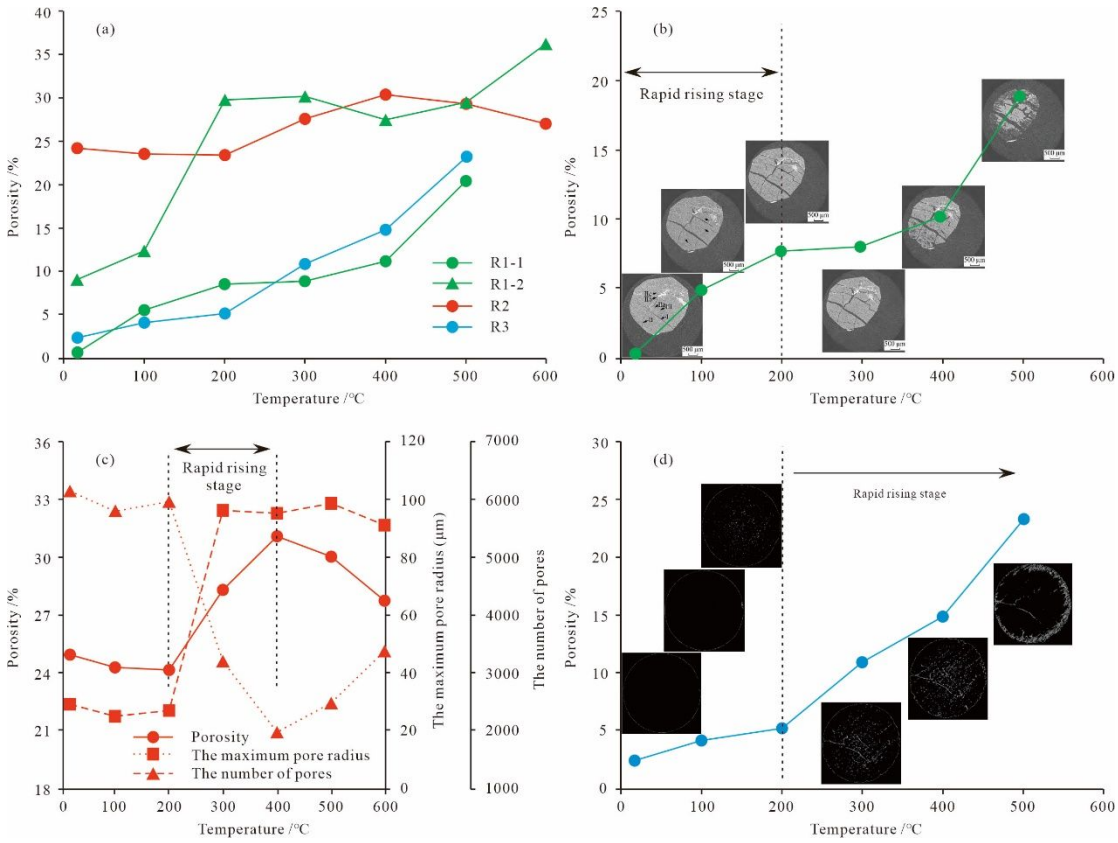

Fig. 11 Porosity evolution pattern of (a) all coal samples, (b) lignite, (c) lean coal, and (d) anthracite at different temperatures. Fig. 11(a) is modified with permission from refs 116-119. Copyright (116)

The medium-rank (R2) coal sample's porosity showed a fluctuating trend of "small decrease–rapid increase–decrease" with increasing temperature. The number of pores and the maximum pore radius decrease slightly with increasing temperature until 200°C, indicating that the matrix expansion effect caused by the increasing temperature dominates at this stage. When the temperature is between 200°C and 400°C, the number of pores decreases, but the maximum pore radius increases considerably, indicating that the coal samples ruptured at this stage. Then, the scale of pores increases after the small-scale pores are connected, and the overall porosity increases significantly. When the temperature exceeds 400°C, the depolymerization and decomposition of coal release a large amount of gas and coal tar to increase the overall porosity, and the coal tar and other products occupy the pore and fracture space after precipitation. The overall porosity decreases again under the coupling of the two effects (Fig. 11(c)).[118]

The porosity of the high-rank coal sample (R3) shows an exponential increase with increasing temperature. Before the temperature reaches 200°C, some water and free gas dissipate to form a few pores, and the coal's porosity increases slightly. When the temperature reaches 300°C, the coal matrix starts to rupture, and numerous pores and fractures are generated in the coal, increasing its overall porosity. As the temperature increases, the number of fractures in the coal increases, the fractures become wider, and the overall porosity increases significantly (Fig. 11(d)).[119]

Comparing the variation laws of pore and fracture structures in coal samples of different coal ranks with temperature changes shows that the porosities of the coal samples during temperature changes are primarily affected by the coupling of the negative effect of matrix expansion caused by the temperature increase, the positive effect of pores and fractures increase caused by gas and water dissipation at the low-temperature stage, and the effects of organic matter pyrolysis at the high-temperature stage. The higher the coal rank (corresponding to higher coal density), the more challenging it is for the coal matrix to rupture. Therefore, the temperature required for the massive generation of pores and fractures in high-rank coal is higher, and the rapid increase stage of porosity in coal occurs later.

5.3 Stress loading

The damage characteristics of coal are closely related to the evolution law of internal microstructures during stress loading, and its study is essential for understanding the stability of coal reservoirs and the fracture development mechanisms under different stress conditions. The deformation and failure of coal occur in four phases: the compaction phase (from O to A), the apparent linear elastic deformation phase (from A to B), the accelerated nonelastic deformation phase (from B to C), and the rupture and development phase (from C to D) (Fig. 12(a)).[32] The evolution of the internal microstructure at different stages can be visualized using the CT testing of key nodes (O, A, B, C, and D) during stress loading. Fig. 12(c) shows that the effective stress in the compaction phase gradually closes the pores and fractures in the coal sample. Then, the pores and fractures remain closed in the linear elastic deformation phase. The coal matrix starts to rupture, and numerous fractures are formed during the accelerated nonelastic deformation phase. During the rupture and development phase, the coal sample's fractures are massively expanded and connected, eventually destroying the

coal sample.[120,121]

The fracture volume and porosity at different phases show a similar evolutionary pattern. The coal's fracture porosity gradually decreases in the compaction phase. Then, the influence of compaction weakens, and the fracture porosity remains stable in the linear elastic deformation phase. In the accelerated nonelastic deformation phase, the coal matrix ruptures, increasing the fracture volume and porosity. Finally, numerous fractures in the coal sample are expanded and connected, rapidly increasing the fracture porosity in the rupture and development phase (Fig. 12(b)).[122,124]

For the loaded coal sample, the surrounding pressure counteracts part of the axial stress and provides some protection to the coal sample. The actual effective stress acting on the sample can be expressed as:

$$\sigma_A = \frac{P_A}{\pi r^2} \times 10 - \frac{\nu}{1-\nu}\left(P_C - P_f\right) \quad (9)$$

where P_A is the applied axial load on coal, MPa; P_c is the confining stress, MPa; r is the radius of coal core (cm); υ is the stationary Poisson's ratio; P_f is fluid pressure in pores and fractures, MPa.

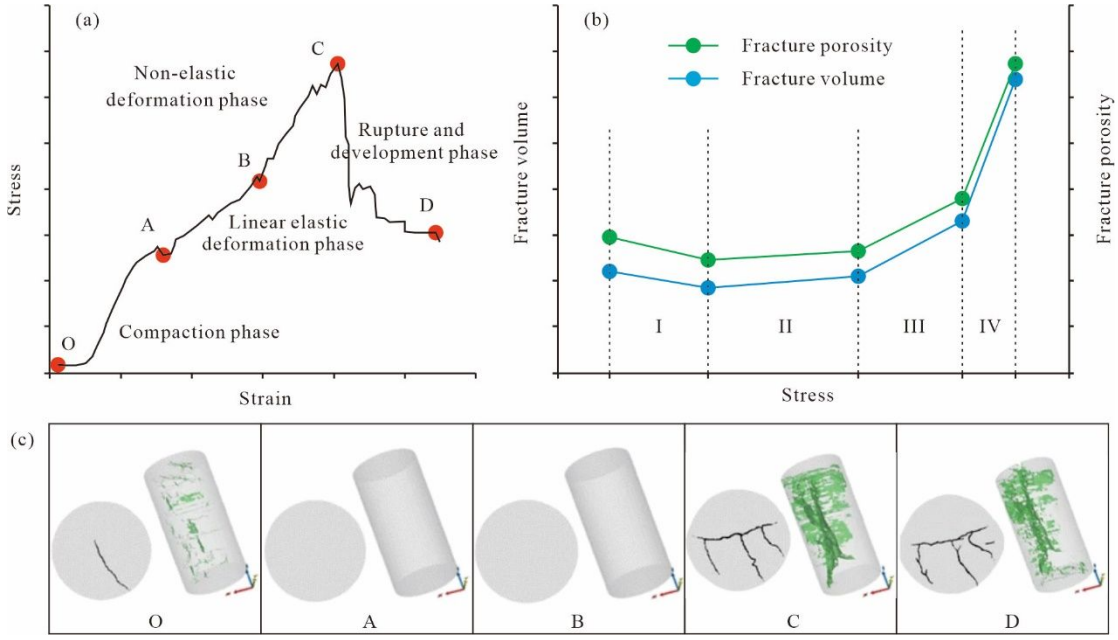

Fig. 12 (a) Stress–strain curve. Modified with permission from ref 123. Copyright 2022 American Chemical Society. (b) Dynamic evolution of fracture volume and fracture porosity during stress loading. Modified with permission from refs 122 and 124. Copyright 2020 and 2022 Elsevier B.V. (c) 3D reconstructed fracture network at different stress loading phases. Modified with permission from ref 121. Copyright 2018 Springer-Verlag GmbH Austria.

Therefore, the higher the surrounding pressure applied to the coal sample, the higher is the axial stress required to destroy the coal sample. The fracture network formed after destroying the coal samples is denser and more complex with the higher surrounding pressure.[121]

Table 3 The specific parameters of each coal sample studied. Table 3 is modified with permission from ref 32. Copyright 2014 Elsevier B.V.

Coal sample ID	D (mm)	L (mm)	$R_{o,m}$ (%)	Density (%)	Uniaxial mechanical properties	
					Young's modulus (MPa)	υ
P1	38.00	77.50	1.94	1.38	2200	0.3
P2	38.49	82.02	2.20	1.40	3610	0.32
P3	38.14	80.85	2.24	1.44	3690	0.21
P4	38.33	82.08	2.68	1.47	4830	0.28
P5	39.04	81.48	3.28	1.68	2270	0.37

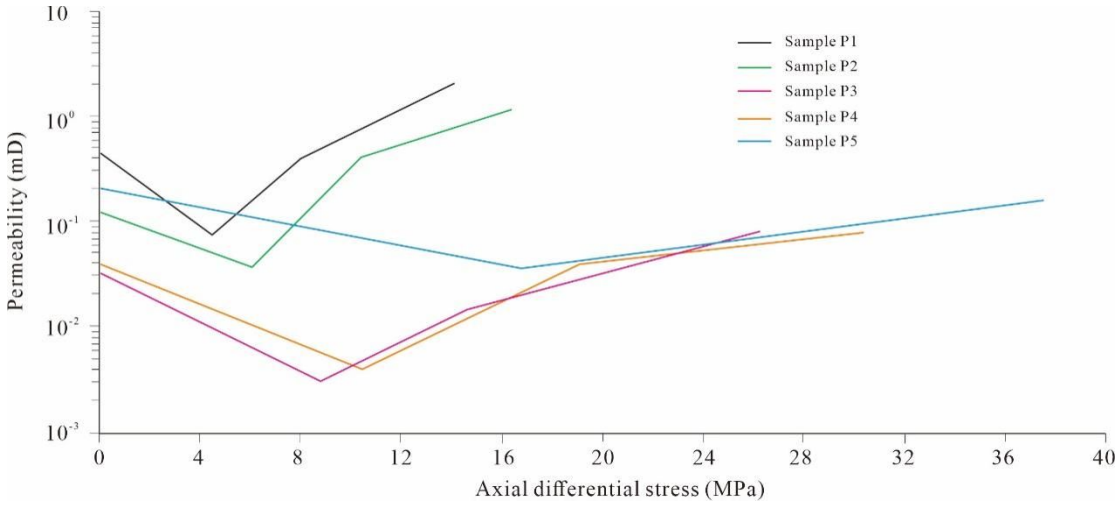

Fig. 13 Evolution of permeability during the deformation of coal samples. Modified with permission from ref 32. Copyright 2014 Elsevier B.V.

The permeability of coal is highly sensitive to stress.[125] By evaluating the permeability of coal samples at the four key nodes O, A, B, and C (the coal sample was damaged at node D, the permeability was substantial and thus not comparable), the evolution of permeability during the deformation of the coal samples can be revealed. Table 3 shows the specific parameters of each coal sample, and Fig. 13 shows the permeability evolution curves. As shown in Fig. 13, the permeability of the coal sample shows a V-shaped evolution law with an increase in the effective stress. The higher the coal sample's degree of metamorphism (corresponding to a higher density), the higher is the peak strength. Thus, the effective stress required for the coal sample to reach the minimum permeability value is higher, and the permeability reduction stage is longer.

6. Challenges and Perspectives

Compared to other testing techniques, CT has the advantages of being nondestructive, characterizing the internal microstructure visually, and constructing 3D structural models. Therefore, this technique is highly favored in coal characterization and has been widely applied in the quantitative characterization of coal microstructures, evaluation of macroscopic properties, and evolutionary mechanisms evaluation of microstructure and macroscopic properties. However, with the increasing applications, the development of this technique has encountered some challenges, and overcoming these challenges is vital to promote the further application of CT in coal characterization. First, the quantitative characterization of microstructures is the basis for understanding coal and conducting macroscopic property evaluations. Due to the limitations of the scanning range and observation accuracy of CT, the accuracy and range of microstructures quantitative characterization cannot be satisfied simultaneously. Moreover, the influence of the model size on pore volumes and porosity interferes with the microstructure characterization results. Currently, CT is mainly used to observer

pores and fractures at the micron level. However, multiscale pores and fractures constitute the fluid storage and transport space in coal. Combining CT with other measurement methods to establish full-scale pore and fracture models is necessary for a finer and comprehensive characterization of the microstructure of coal samples, which is more conducive to guiding the study of gas adsorption, diffusion, and seepage properties in coal.

Second, when evaluating macroscopic properties based on the microstructures of coal, the influence mechanism of pores and fractures on macroscopic properties is primarily considered. However, minerals are a component of the coal skeleton and play an equally crucial role in defining coal properties. The mineral content, particle size distribution, and complexity of coal can be quantitatively characterized using CT, but the mineral types cannot be distinguished. There are differences in the composition, water absorption, and stress sensitivity of different minerals, which can directly affect the changes in the porosity, permeability, and mechanical properties of coal during wetting, stressing, and chemical treatment. Identifying different mineral types in the microstructure of coal allows for a finer evaluation of its macroscopic properties.

Finally, as the application of CT in coal characterization gradually evolves from static to dynamic, the dynamic evolution of microstructure and macroscopic properties under different effects becomes a crucial development trend. In addition to the effects of gas adsorption, temperature change, and stress loading, future research also has more significant advantages in explaining the transport and blockage mechanisms of solid particles in coal fractures, and the influence of liquid (water or acid solution) content and contact time on the microstructure and permeability of coal. Furthermore, the CT test process is complicated and expensive; therefore, this technology cannot be widely used as a conventional method. Thus, selecting the key points of the dynamic evolution

process of microstructure and macroscopic properties is critical for achieving better research results.

7. Conclusions

In this study, we introduced the principle of CT imaging and microstructure recognition. The methods of coal microstructure characterization and macroscopic property evaluation using CT are summarized. Furthermore, the applications of CT in studying the evolution mechanism of coal microstructure and macroscopic properties during gas adsorption, temperature change, and damage deformation are discussed. Based on our comprehensive review, the following conclusions are obtained.

1) Although several methods are available for the effective characterization and quantification of coal microstructure, CT can be used to reconstruct a 3D microstructure model, and its application in coal microstructure characterization is indispensable.

2) By establishing the relationship between microstructure and macroscopic properties, CT can be used to evaluate the macroscopic properties of coal, including its porosity, gas adsorption/diffusion rate, permeability, and mechanical properties.

3) By visualizing the evolution of the pore and fracture structures, porosity, and permeability of the coal sample at various stages of gas adsorption, temperature change, and stress loading, CT provides a feasible method to study the mechanism of coal matrix deformation and its effects on microstructure and macroscopic properties.

4) CT technology faces limitations, such as a small scanning range, limited observation accuracy, functional limitations, lengthy testing process, and high cost, which present hurdles in the broad application of CT in coal characterization. In the future, it should be combined with other techniques to establish full-scale pore and fracture models, identify the mineral types in microstructures, and effusively use the advantages of CT by selecting the key points in the evolutionary mechanisms of microstructure and

macroscopic properties.

Conflicts of Interest

The authors declare no competing financial interest.

Acknowledgments

This research was funded by the National Natural Science Foundation of China (grant nos. 42130806, 41830427, 41922016 and 42102227).

Biographies

Dameng Liu

Dameng Liu received his bachelor's degree from Xiangtan Mining Institute and obtained his Ph.D. degree from China University of Mining and Technology (Beijing). He is a professor and serves as vice president of China University of Geosciences (Beijing). He is mainly engaged in the research of coal measure gas geology theory and evaluation technology.

Zheng Zhao

Zheng Zhao graduated from Henan Polytechnic University with a bachelor's degree, and is currently studying for a Ph.D. degree in geological exploration and development at China University of Geosciences (Beijing). He is mainly engaged in the research of coal measure gas geology and development.

Yidong Cai

Yidong Cai graduated from China University of Geosciences (Beijing) and obtained his Ph.D. degree in geological exploration and development. He is a professor in the School of Energy Resources, China University of Geosciences (Beijing). He is mainly engaged in the research of coal measure gas geology and development.

Fengrui Sun

Fengrui Sun received his bachelor's degree from China University of Petroleum (East

China) and obtained his Ph.D. degree from China University of Petroleum (Beijing). He is currently doing postdoctoral research at China University of Geosciences (Beijing), and has been engaged in the research of wellbore multiphase flow for a long time.

Yingfang Zhou

Yingfang Zhou received his bachelor's degree from China University of Geosciences (Beijing) and obtained his Ph.D. degree from the University of Stavanger. He is an associate professor at the University of Aberdeen and has been working on wettability characterization, reservoir modeling, and CO_2 geological storage for several years.

References

(1) Liu, D.M.; Zou, Z.; Cai, Y.D.; Qiu, Y.K.; Zhou, Y.F.; He, S. An updated study on CH_4 isothermal adsorption and isosteric adsorption heat behaviors of variable rank coals. J. Nat. Gas Sci. Eng. **2021**, 89, 103899.

(2) Cai, Y.D.; Liu, D.M.; Pan, Z.J.; Che, Y.; Liu, Z.H. Investigating the effects of seepage-pores and fractures on coal permeability by fractal analysis. *Transport Porous Med*. **2016**, 111(2), 479-497.

(3) Zhou, S.D.; Liu, D.M.; Cai, Y.D.; Wang, Y.J.; Yan, D.T. Mineral characteristics of low-rank coal and the effects on the micro- and nanoscale pore-fractures: A case study from the Zhundong Coalfield, Northwest China. *J. Nanosci. Nanotechno.* **2021**, 21(1 S1), 460-471.

(4) Han, W.B.; Zhou, G.; Gao, D.H.; Zhang, Z.X.; Wei, Z.Y.; Wang, H.T.; Yang, H.Q. Experimental analysis of the pore structure and fractal characteristics of different metamorphic coal based on mercury intrusion-nitrogen adsorption porosimetry. *Powder Technol.* **2020**, 362, 386-398.

(5) Zhao, Z.; Ni, X.M.; Cao, Y.X.; Shi, Y.X. Application of fractal theory to predict the coal permeability of multi-scale pores and fractures. *Energy Rep.* **2021**, 7, 10-18.

(6) Liu, Z.S.; Liu, D.M.; Cai, Y.D.; Qiu, Y.K. Permeability, mineral and pore characteristics of coals response to acid treatment by NMR and QEMSCAN: Insights into acid sensitivity mechanism. *J. Petrol. Sci. Eng.* **2021**, 198, 108205.

(7) Yao, Y.B.; Liu, D.M. Comparison of low-field NMR and mercury intrusion porosimetry in characterizing pore size distributions of coals. *Fuel* **2012**, 95, 152-158.

(8) Okolo, G.N.; Everson, R.C.; Neomagus, H.W.J.P.; Roberts, M.J.; Sakurovs, R. Comparing the porosity and surface areas of coal as measured by gas adsorption, mercury intrusion and SAXS techniques. *Fuel* **2015**, 141, 293-304.

(9) Li, Y.; Wang, Z.S.; Pan, Z.J.; Niu, X.L.; Yu, Y.; Meng, S.Z. Pore structure and its fractal dimensions of transitional shale: A cross-section from east margin of the Ordos Basin, China. *Fuel* **2019**, 241, 417-431.

(10) Xu, H.; Tang, D.Z.; Chen, Y.P.; Ming, Y.; Chen, X.Y.; Qu, H.X.; Yuan, Y.X.; Li, S.; Tao, S. Effective porosity in lignite using kerosene with low-field nuclear magnetic resonance. *Fuel* **2018**, 213, 158-163.

(11) Nie, B.S.; Liu, X.F.; Yang, L.L.; Meng, J.Q.; Li, X.C. Pore structure characterization of different rank coals using gas adsorption and scanning electron microscopy. *Fuel* **2015**, 158, 908-917.

(12) Li, Y.; Yang, J.H.; Pan, Z.J.; Tong, W.S. Nanoscale pore structure and mechanical property analysis of coal: An insight combining AFM and SEM images. *Fuel* **2020**, 260, 116352.

(13) Li, Y.; Chen, J.Q.; Yang, J.H.; Liu, J.S.; Tong, W.S. Determination of shale macroscale modulus based on microscale measurement: A case study concerning multiscale mechanical characteristics. *Petrol. Sci.* **2021**, https://doi.org/10.1016/j.petsci.2021.10.004.

(14) Cui, J.; Liu, D.M.; Cai, Y.D.; Pan, Z.J.; Zhou, Y.F. Insights into fractures and minerals in subbituminous and bituminous coals by FESEM-EDS and X-ray mu-CT. *Fuel* **2019**, 237, 977-988.

(15) Zhang, L.; Chen, S.; Zhang, C.; Fang, X.Q.; Li, S. The characterization of bituminous coal microstructure and permeability by liquid nitrogen fracturing based on μ-CT technology. *Fuel* **2020**, 262, 116635.

(16) Li, Y., Tang, D., Elsworth, D., Xu, H. Characterization of coalbed methane reservoirs at multiple length scales: a cross-section from southeastern Ordos Basin, China. *Energy & Fuels*, **2014**, 28(9): 5587-5595.

(17) Zhang, K.Z.; Cheng, Y.P.; Li, W.; Hao, C.M.; Hu, B.; Jiang, J.Y. Microcrystalline characterization and morphological structure of tectonic anthracite using XRD, liquid nitrogen adsorption, mercury porosimetry, and micro-CT. *Energy Fuels* **2019**, 33(11), 10844-10851.

(18) Kemp, C.N. The X-Ray examination of coal sections. *P. Roy. Soc. Edinb.* **1929**, 48, 167-179.

(19) Hayashizaki, H.; Kubota, Y.; Arima, T.; Uebo, K.; Nomura, S. Observation of the coal thermoplastic layer using μ-focus X-ray CT and sole-heated oven. *ISIJ Int.* **2014**, 54(11), 2477-2483.

(20) Pan, J.N.; Niu, Q.H.; Wang, K.; Shi, X.H.; Li, M. The closed pores of tectonically deformed coal studied by small-angle X-ray scattering and liquid nitrogen adsorption. *Micropor. Mesopor. Mat.* **2016**, 224, 245-252.

(21) Li, Q.; Liu, D.M.; Cai, Y.D.; Zhao, B.; Qiu, Y.K. Zhou, Y.F. Scale-span pore structure heterogeneity of high volatile bituminous coal and anthracite by FIB-SEM and X-ray mu-CT. *J. Nat. Gas Sci. Eng.* **2020**, 81, 103443.

(22) Wang, G.; Han, D.Y.; Jiang, C.H.; Zhang, Z.Y. Seepage characteristics of fracture and dead-end pore structure in coal at micro- and meso-scales. *Fuel* **2020**, 266, 117058.

(23) Mathews, J.P.; Campbell, Q.P.; Xu, H.; Halleck, P. A review of the application of X-ray computed tomography to the study of coal. *Fuel* **2017**, 209, 10-24.

(24) Mostaghimi, P.; Armstrong, R.T.; Gerami, A.; Hu, Y.B.; Jing, Y.; Kamali, F.; Liu, M.; Liu, Z.S.; Lu, X.; Ramandi, H.L.; Zamani, A.; Zhang, Y.L. Cleat-scale characterisation of coal: An overview. *J. Nat. Gas Sci. Eng.* **2017**, 39, 143-160.

(25) Johns, R.A.; Steude, J.S.; Castanier, L.M.; Roberts, P.V. Nondestructive measurements of fracture aperture in crystalline rock cores using X-ray computed tomography. *J. Geophys. Res-Sol. Ea.* **1993**, 98(B2), 1889-1900.

(26) Wang, B.; Wu, Y.T.; Li, G.F.; Yang, J.S.; Zhao, Y.; Wang, M.Z.; Zhou, J.; Wu, T.; Pan, Z.J. Laboratory study of fracture permeability of mineral-filled coal from Fanzhuang Block, southern Qinshui Basin, China. *J. Petrol. Sci. Eng.* **2022**, 208, 109799.

(27) Yang, S.Q.; Ranjith, P.G.; Jing, H.W.; Tian, W.L.; Ju, Y. An experimental investigation on thermal damage and failure mechanical behavior of granite after exposure to different high temperature treatments. *Geothermics* **2017**, 65, 180-197.

(28) Jackson, D.F.; Hawkes, D.J. X-ray attenuation coefficients of elements and mixtures. *Phys. Rep.* **1981**, 70(3), 169–233.

(29) Chakraborty, N.; Lou, X.Q.; Enab, K.; Karpyn, Z. Measurement of in-situ fluid density in shales with sub-resolution porosity using X-Ray microtomography. *Transport Porous Med.* **2022**, 141(3), 607-627.

(30) Zhou, H.W.; Zhong, J.C.; Ren, W.G.; Wang, X.Y.; Yi, H.Y. Characterization of pore-fracture networks and their evolution at various measurement scales in coal samples using X-ray μ-CT and a fractal method. *Int. J. Coal. Geol.* **2018**, 189, 35-49.

(31) Wang, G.; Shen, J.N.; Liu, S.M.; Jiang, C.H.; Qin, X.J. Three-dimensional modeling and analysis of macro-pore structure of coal using combined X-ray CT imaging and fractal theory. *Int. J. Rock Mech. Min.* **2019**, 123, 104082.

(32) Cai, Y.D.; Liu, D.M.; Mathews, J.P.; Pan, Z.J.; Elsworth, D.; Yao, Y.B.; Li, J.Q.; Guo, X.Q. Permeability evolution in fractured coal-combining triaxial confinement with X-ray computed tomography, acoustic emission and ultrasonic techniques. *Int. J. Coal. Geol.* **2014**, 122, 91-104.

(33) Cai, T.T.; Feng, Z.C.; Zhou, D. Multi-scale characteristics of coal structure by X-ray computed tomography (X-ray CT), scanning electron microscope (SEM) and mercury intrusion porosimetry (MIP). *AIP Adv.* **2018**, 8(2), 025324.

(34) Du, F.; Wang, K.; Zhang, G.J.; Zhang, Y.; Zhang, G.D.; Wang, G.D. Damage characteristics of coal under different loading modes based on CT three-dimensional reconstruction. *Fuel* **2022**, 310, 122304.

(35) Lu, Y.J.; Liu, D.M.; Cai, Y.D.; Li, Q.; Zhou, Y.F. Spontaneous imbibition in coal with in-situ dynamic micro-CT imaging. *J. Petrol. Sci. Eng.* **2022**, 208, 109296.

(36) Zhang, K.Z.; Wang, S.L.; Wang, L.; Cheng, Y.P.; Li, W.; Han, X.W.; Liu, C.; Su, H.R. 3D visualization of tectonic coal microstructure and quantitative characterization on topological connectivity of pore-fracture networks by Micro-CT. *J. Petrol. Sci. Eng.* **2022**, 208, 109675.

(37) Jing, Y.; Armstrong, R.T.; Ramandi, H.L.; Mostaghimi, P. Topological characterization of fractured coal. *J. Geophys. Res-Sol. Ea.* **2017**, 122(12), 9849-9861.

(38) Pant, L.M.; Huang, H.P.; Secanell, M.; Larter, S.; Mitra, S.K. Multi scale characterization of coal structure for mass transport. *Fuel* **2015**, 159, 315-323.

(39) Akhondzadeh, H.; Keshavarz, A.; Al-Yaseri, A.Z.; Ali, M.; Awan, F.U.R.; Wang, X.; Yang, Y.F.; Iglauer, S.; Lebedev, M. Pore-scale analysis of coal cleat network evolution through liquid nitrogen treatment: A micro-computed tomography investigation. *Int. J. Coal. Geol.* **2020**, 219, 103307.

(40) Han, L.; Shen, J.; Qu, J.; Ji, C.J. Characteristics of a multi-scale fracture network and its contributions to flow properties in anthracite. *Energy Fuels* **2021**, 35(14): 11319-11332.

(41) Zhu, Q.Z.; Wang, X.L.; Zuo, Y.Q.; Pan, J.N.; Ju, Y.W.; Su, X.F.; Yu, K. Numerical simulation of matrix swelling and its effects on fracture structure and permeability for a high-rank coal based on X-ray micro-CT image processing techniques. *Energy Fuels* **2020**, 34(9): 10801-10809.

(42) Wang, G.; Qin, X.J.; Shen, J.N.; Zhang, Z.Y.; Han, D.Y.; Jiang, C.H. Quantitative analysis of microscopic structure and gas seepage characteristics of low-rank coal based on CT three-dimensional

reconstruction of CT images and fractal theory. *Fuel* **2019**, 256, 115900.

(43) Fan, N.; Wang, J.R.; Deng, C.B.; Fan, Y.P.; Wang, T.T.; Guo, X.Y. Quantitative characterization of coal microstructure and visualization seepage of macropores using CT-based 3D reconstruction. *J. Nat. Gas Sci. Eng.* **2020**, 81, 103384.

(44) Wei, J.P.; Li, B.; Wang, K.; Sun, D.H. 3D numerical simulation of boreholes for gas drainage based on the pore-fracture dual media. *Int. J. Min. Sci. Techno.* **2016**, 26(4), 739-744.

(45) Mukherjee, M.; Misra, S. A review of experimental research on enhanced coal bed methane (ECBM) recovery via CO_2 sequestration. *Earth-Sci. Rev.* **2018**, 179, 392-410.

(46) Chen, W.X.; He, X.Q.; Liu, M.J.; Mitri, H.; Wang, Q. Meso- and macro-behaviour of coal rock: observations and constitutive model development. *Int. J. Min. Reclam. Env.* **2016**, 30(1), 13-24.

(47) Liu, D.M.; Yao, Y.B.; Tang, D.Z.; Tang, S.H.; Che, Y.; Huang, W.H. Coal reservoir characteristics and coalbed methane resource assessment in Huainan and Huaibei coalfields, Southern North China. *Int. J. Coal. Geol.* **2009**, 79(3), 97-112.

(48) Ni, X.M.; Miao, J.; Lv, R.S.; Lin, X.Y. Quantitative 3D spatial characterization and flow simulation of coal macropores based on mu CT technology. *Fuel* **2017**, 200, 199-207.

(49) Li, Z.T.; Liu, D.M.; Cai, Y.D.; Ranjith, P.G.; Yao, Y.B. Multi-scale quantitative characterization of 3-D pore-fracture networks in bituminous and anthracite coals using FIB-SEM tomography and X-ray μ-CT. *Fuel* **2017**, 209: 43-53.

(50) Wang, X.L.; Pan, J.N.; Wang, K.; Ge, T.Y.; Wei, J.; Wu, W. Characterizing the shape, size, and distribution heterogeneity of pore-fractures in high rank coal based on X-ray CT image analysis and mercury intrusion porosimetry. *Fuel* **2020**, 282, 118754.

(51) Peng, R.D.; Yang, Y.C.; Ju, Y.; Miao, L.T.; Yang, Y.M. Computation of fractal dimension of rock pores based on gray CT images. *Chin. Sci. Bull.* **2011**, 56(31), 3346-3357.

(52) Liu, P.; Ju, Y.; Ranjith, P.G.; Zheng, Z.M.; Chen, J.L. Experimental investigation of the effects of heterogeneity and geostress difference on the 3D growth and distribution of hydrofracturing cracks in unconventional reservoir rocks. *J. Nat. Gas Sci. Eng.* **2016**, 35, 541-554.

(53) Ding, Y.; Weller, A.; Zhang, Z.; Kassab, M. Fractal dimension of pore space in carbonate samples from Tushka area (Egypt). *Arab. J. Geosci.* **2017**, 10(17), 388.

(54) Fu, H.J.; Tang, D.Z.; Xu, T.; Xu, H.; Tao, S.; Li, S.; Yin, Z.Y.; Chen, B.L.; Zhang, C.; Wang, L.L. Characteristics of pore structure and fractal dimension of low-rank coal: A case study of Lower Jurassic

Xishanyao coal in the southern Junggar Basin, NW China. *Fuel* **2017**, 193, 254-264.

(55) Wu, H.; Yao, Y.B.; Zhou, Y.F.; Qiu, F. Analyses of representative elementary volume for coal using X-ray μ-CT and FIB-SEM and its application in permeability predication model. *Fuel* **2019**, 254, 115563.

(56) Ai, T.; Zhang, R.; Zhou, H.W.; Pei, J.L. Box-counting methods to directly estimate the fractal dimension of a rock surface. *Appl. Surf. Sci.* **2014**, 314, 610-621.

(57) Shi, X.H.; Pan, J.N.; Hou, Q.L.; Jin, Y.; Wang, Z.Z.; Niu, Q.H.; Li, M. Micrometer-scale fractures in coal related to coal rank based on micro-CT scanning and fractal theory. *Fuel* **2018**, 212, 162-172.

(58) Gerami, A.; Mostaghimi, P.; Armstrong, R.T.; Zamani, A.; Warkiani, M.E. A microfluidic framework for studying relative permeability in coal. *Int. J. Coal. Geol.* **2016**, 159, 183-193.

(59) Shi, X.H.; Pan, J.N.; Pang, L.L.; Wang, R.; Li, G.F.; Tian, J.J, Wang, H.C. 3D microfracture network and seepage characteristics of low-volatility bituminous coal based on nano-CT. *J. Nat. Gas Sci. Eng.* **2020**, 83, 103556.

(60) Wang, J.Y.; Jiang, F.J.; Zhang, C.L.; Song, Z.Z.; Mo, W.L. Study on the pore structure and fractal dimension of tight sandstone in coal measures. *Energy Fuels* **2021**, 35(5), 3887-3898.

(61) Silin. D.; Patzek, T. Pore space morphology analysis using maximal inscribed spheres. *Physica A.* **2006**, 371(2), 336-360.

(62) Dong, H.; Blunt, M.J. Pore-network extraction from micro-computerized-tomography images. *Phys. rev. E* **2009**, 80(3 Pt 2), 036307.

(63) Feng, Z.Z.; Zhao, Y.S.; Duan, K.L. Influence of rock cell characteristic and rock inhomogeneity parameter on complete curve of stress-strain. *Chin. J. Rock Mech. Eng.* **2004**, 23(11), 1819-1823.

(64) Fu, Y.; Feng, Z.L.; Li, P.C. Heterogeneous characteristics of coal based on CT scanning and numerical analysis of its reconstruction model. *J. Min. Safety Eng.* **2020**, 37(04), 828-835.

(65) Fu, Y., Feng, Z.L. Simulation of the effect of coal microstructures on the macroscopic mechanical behavior. *Adv. Civ. Eng.* **2020**, 2020, 1025952.

(66) Cai, J.C.; Xia, Y.X.; Lu, C.; Bian, H.; Zou, S.M. Creeping microstructure and fractal permeability model of natural gas hydrate reservoir. *Mar. Petrol. Geol.* **2020**, 115, 104282.

(67) Liu, W.; Wang, G.; Han, D.Y.; Xu, Hao.; Chu, X.Y. Accurate characterization of coal pore and fissure structure based on CT 3D reconstruction and NMR. *J. Nat. Gas Sci. Eng.* **2021**, 96, 104242.

(68) Garum, M.; Glover, P.W.J.; Lorinczi, P.; Drummond-Brydson, R.; Hassanpour, A. Micro- and nano-scale pore structure in gas shale using X mu-CT and FIB-SEM techniques. *Energy Fuels* **2020**, 34(10),

12340-12353.

(69) Zhang, Y.L.; Mostaghimi, P.; Fogden, A.; Sheppard, A.; Arena, A.; Middleton, J.; Armstrong, R.T. Time-lapsed visualization and characterization of shale diffusion properties using 4D X-ray microcomputed tomography. *Energy Fuels* **2018**, 32(3), 2889-2900.

(70) Cai, Y.D.; Liu, D.M.; Pan, Z.J.; Yao, Y.B.; Li, J.Q.; Qiu, Y.K. Pore structure and its impact on CH_4 adsorption capacity and flow capability of bituminous and subbituminous coals from Northeast China. *Fuel* **2013**, 103, 258-268.

(71) Wei, Q.; Li, X.Q.; Zhang, J.Z.; Hu, B.L.; Zhu, W.W.; Lian, W.L.; Sun, K.X. Full-size pore structure characterization of deep-buried coals and its impact on methane adsorption capacity: A case study of the Shihezi Formation coals from the Panji deep area in Huainan Coalfield, Southern North China. *J. Petrol. Sci. Eng.* **2019**, 173, 975-989.

(72) Karacan, C.O.; Okandan, E. Adsorption and gas transport in coal microstructure: investigation and evaluation by quantitative X-ray CT imaging. *Fuel* **2001**, 80(4), 509-520.

(73) Mayo, S.; Josh, M.; Kasperczyk, D.; Rear, J.; Zhang, J.F.; Dautriat, J.; Pervukhina, M.; Ben Clennell, M.; Sakurovs, R.; Sherwood, N.; Maksimenko, A.; Hall, C. Dynamic micro-CT study of gas uptake in coal using Xe, Kr and CO_2. *Fuel* **2018**, 212, 140-150.

(74) Zhou, D.; Feng, Z.C.; Zhao, D.; Zhao, Y.S.; Cai, T.T. Uniformity of temperature variation in coal during methane adsorption. *J. Nat. Gas Sci. Eng.* **2016**, 33, 954-960.

(75) Feng, Z.C.; Cai, T.T.; Zhou, D.; Zhao, D.; Zhao, Y.S.; Wang, C. Temperature and deformation changes in anthracite coal after methane adsorption. *Fuel* **2017**, 192, 27-34.

(76) Seomoon, H.; Lee, M.; Sung, W. Analysis of sorption-induced permeability reduction considering gas diffusion phenomenon in coal seam reservoir. *Transport. Porous Med.* **2015**, 108(3), 713-729.

(77) Sun, Y.F.; Zhao, Y.X.; Yuan, L. CO_2-ECBM in coal nanostructure: Modelling and simulation. *J. Nat. Gas Sci. Eng.* **2018**, 54, 202-215.

(78) Fang, H.H.; Xu, H.J.; Sang, S.X.; Liu, S.Q.; Song, S.L.; Liu, H.H. 3D reconstruction of coal pore network and its application in CO_2-ECBM process simulation at laboratory scale. *Front. Earth Sci.* **2021**. DOI: 10.1007/s11707-021-0944-3.

(79) Fang, H.H.; Sang, S.X.; Liu, S.Q. Three-dimensional spatial structure of the macro-pores and flow simulation in anthracite coal based on X-ray μ-CT scanning data. *Petrol. Sci.* **2020**, 17(5), 1221-1236.

(80) Jing, Y.; Armstrong, R.T.; Mostaghimi, P. Impact of mineralization on digital coal properties.

Energy Fuels **2017**, 31(11), 11558-11568.

(81) Fang, H.H.; Sang, S.X.; Du, Y.; Liu, H.H.; Xu, H.J. Visualization characterization of minerals touched by interconnected pores and fractures and its demineralization effect on coal permeability during CO_2-ECBM process based on X-ray CT data. *J. Nat. Gas Sci. Eng.* **2021**, 95, 104213.

(82) Chen, J.; Cheng, W.M.; Wang, G.; Li, H.M. Effect of dominated coal pores and fractures on water migration after low-pressure water injection based on CT images. *Fuel* **2022**, 307, 121795.

(83) Jing, D.J.; Meng, X.X.; Ge, S.C.; Zhang, T.; Ma, M.X.; Tong, L.Q. Reconstruction and seepage simulation of a coal pore-fracture network based on CT technology. *Plos One* **2021**, 16(6), e0252277.

(84) Li, S.; Tang, D.Z.; Xu, H.; Yang, Z. Advanced characterization of physical properties of coals with different coal structures by nuclear magnetic resonance and X-ray computed tomography. *Comput. Geosci.* **2012**, 48, 220-227.

(85) Wang, G.; Yang, X.X.; Chu, X.Y.; Shen, J.N.; Jiang, C.H. Microscale numerical simulation of non-Darcy flow of coalbed methane. *Arab. J. Sci. Eng.* **2018**, 43(5), 2547-2561.

(86) Liu, D.; Zhou, G.; Miao, Y.N.; Guo, S.J.; Zhang, J.Q. Numerical simulation investigation for stress deformation and water injection seepage of coal microstructure under uniaxial compression. *J. Energ. Eng.* **2021**, 147(5): 04021036.

(87) Ramandi, H.L.; Mostaghimi, P.; Armstrong, R.T.; Saadatfar, M.; Pinczewski, W.V. Porosity and permeability characterization of coal: a micro-computed tomography study. *Int. J. Coal. Geol.* **2016**, 154, 57-68.

(88) Yao, Y.B.; Liu, D.M.; Cai, Y.D.; Li, J.Q.; Advanced characterization of pores and fractures in coals by nuclear magnetic resonance and X-ray computed tomography. *Sci. China Earth Sci.* **2010**, 53(6), 854-862.

(89) Ramandi, H.L.; Liu, M.; Tadbiri, S.; Mostaghimi, P. Impact of dissolution of syngenetic and epigenetic minerals on coal permeability. *Chem. Geol.* **2018**, 486, 31-39.

(90) Li, X.; Fu, X.H.; Tian, J.J.; Guan, W.M.; Liu, X.L.; Ge, Y.Y.; Ranjith, P.G.; Wang, W.F.; Wang, M.; Liang, S. Heterogeneities of seepage pore and fracture of high volatile bituminous coal core: Implications on water invasion degree. *J. Petrol. Sci. Eng.* **2019**, 183, 106409.

(91) Lv, Z.X.; Ji, Q.Q.; Ren, W.J. Experimental study and percolation analysis on seepage characteristics of fractured coal and sandstone based on real-time micro-CT. *Geofluids* **2020**, 2020, 8832946.

(92) Zhang, X.Q.; Wang, K.; Wang, A.; Gong, P.L. Analysis of internal pore structure of coal by micro-

computed tomography and mercury injection. *Int. J. Oil Gas Coal T.* **2016**, 12(1), 38-50.

(93) Zhao, Y.X.; Song, H.H.; Liu, S.M.; Zhang, C.G.; Dou, L.M.; Cao, A.Y. Mechanical anisotropy of coal with considerations of realistic microstructures and external loading directions. *Int. J. Rock Mech. Min.* **2019**, 116, 111-121.

(94) Cheng, M.; Fu, X.H.; Kang, J.Q. Compressibility of different pore and fracture structures and its relationship with heterogeneity and minerals in low-rank coal reservoirs: an experimental study based on nuclear magnetic resonance and micro-CT. *Energy Fuels* **2020**, 34(9), 10894-10903.

(95) Cai, Y.D.; Liu, D.M.; Pan, Z.J.; Yao, Y.B.; Li, C.C. Mineral occurrence and its impact on fracture generation in selected Qinshui Basin coals: An experimental perspective. *Int. J. Coal. Geol.* **2015**, 150, 35-50.

(96) Zhao, Y.X.; Liu, S.M.; Zhao, G.F.; Elsworth, D.; Jiang, Y.D.; Han, J.L. Failure mechanisms in coal: Dependence on strain rate and microstructure. *J. Geophys. Res-Sol. Ea.* **2014**, 119(9), 6924-6935.

(97) Chen, S.D.; Tang, D.Z.; Tao, S.; Ji, X.Y.; Xu, H. Fractal analysis of the dynamic variation in pore-fracture systems under the action of stress using a low-field NMR relaxation method: An experimental study of coals from western Guizhou in China. *J. Petrol. Sci. Eng.* **2019**, 173, 617-629.

(98) Hou, L.L.; Liu, X.J.; Liang, L.X.; Zhang, P.; Xie, B.; Li, D.Q. Numerical simulation of effect of cleats on energy evolution of coal and rock in loading process. *J. China Coal Soc.* **2020**, 45(03), 1061-1069.

(99) Steel, K.M.; Dawson, R.E.; Jenkins, D.R.; Pearce, R.; Mahoney, M.R. Use of rheometry and micro-CT analysis to understand pore structure development in coke. *Fuel Process. Technol.* **2017**, 155, 106-113.

(100) Li, Y.T.; Guo, Q.W.; Liu, X.C.; Jiang, Y.D.; Zhang, B.; Wang, H. Investigation on pore-fracture of coal and its influence mechanism on tensile failure behavior of coals with bursting proneness. *Geofluids* **2021**, 2021, 7574305.

(101) Cao, W.Z.; Yildirim, B.; Durucan, S.; Wolf, K.H.; Cai, W.; Wolf, K.H.; Korre, A. Fracture behaviour and seismic response of naturally fractured coal subjected to true triaxial stresses and hydraulic fracturing. *Fuel* **2021**, 288, 119618.

(102) Akhondzadeh, H.; Keshavarz, A.; Awan, F.U.R.; Ali, M.; Al-Yaseri, A.; Liu, C.F.; Yang, Y.F.; Iglauer, S.; Gurevich, B.; Lebedev, M. Liquid nitrogen fracturing efficiency as a function of coal rank: A multi-scale tomographic study. *J. Nat. Gas Sci. Eng.* **2021**, 95, 104177.

(103) Gong, S. Investigation of tensile and fracture mechanical properties of bituminous coal at different strain rates. *J. Mater. Res. Technol.* **2021**, 15, 834-845.

(104) Ding, X.; Xiao, X.C.; Lv, X.F.; Wu, D.; Xu, J. Mechanical properties of bump-prone coal with different porosities and its acoustic emission-charge induction characteristics under uniaxial compression. *Adv. Civ. Eng.* **2019**, 2019, 7581061.

(105) Wu, Y.N.; Zhang, Z.; Wang, X.Z.; Zhu, P.Y.; Yang, X.; Jiang, L.S. Study on the physical properties and joint evolution characteristics of three-dimensional reconstructed coal. *Adv. Mater. Sci. Eng.* **2021**, 2021, 7038110.

(106) Nie, X.R.; Chen, J.B.; Cao, Y.; Gong, D.G.; Deng, H. Analysis of coal swelling deformation caused by carbon dioxide adsorption based on X-Ray computed tomography. *Geofluids* **2018**, 2018, UNSP 6939827.

(107) Karacan, C.O.; Mitchell, G.D. Behavior and effect of different coal microlithotypes during gas transport for carbon dioxide sequestration into coal seams. *Int. J. Coal. Geol.* **2003**, 53(4), 201-217.

(108) Wei, M.Y.; Liu, J.S.; Liu, Y.K.; Liu, Z.H.; Elsworth, D. Effect of adsorption-induced matrix swelling on coal permeability evolution of micro-fracture with the real geometry. *Petrol. Sci.* **2021**, 18(4), 1143-1152.

(109) Zhou, D.; Liu, Z.X.; Feng, Z.C.; Shen, Y.X.; Wu, Y.C. The study of the local area density homogenization effect of meso-structures in coal during methane adsorption. *J. Petrol. Sci. Eng.* **2020**, 191, 107141.

(110) Feng, Z.C.; Zhou, D.; Zhao, Y.S.; Cai, T.T. Study on microstructural changes of coal after methane adsorption. *J. Nat. Gas Sci. Eng.* **2016**, 30, 28-37.

(111) Zhou, D.; Feng, Z.C.; Zhao, D.; Zhao, Y.S.; Cai, T.T. Experimental study of meso-structural deformation of coal during methane adsorption-desorption cycles. *J. Nat. Gas Sci. Eng.* **2017**, 42, 243-251.

(112) Lan, W.J.; Wang, H.X.; Zhang, X.; Fan, H.B.; Feng, K.; Liu, Y.X.; Sun, B.Y. Investigation on the mechanism of micro-cracks generated by microwave heating in coal and rock. *Energy* **2020**, 206, 118211.

(113) Wang, D.K.; Zhang, P.; Wei, J.P.; Yu, C. The seepage properties and permeability enhancement mechanism in coal under temperature shocks during unloading confining pressures. *J. Nat. Gas Sci. Eng.* **2020**, 77, 103242.

(114) Zhang, H.T.; Wang, D.K.; Yu, C.; Wei, J.P.; Liu, S.M.; Fu, J.H. Microcrack evolution and

permeability enhancement due to thermal shocks in coal. *Plos One* **2020**, 15(5), e0232182.

(115) Wen, H.; Wei, G.M.; Ma, L.; Li, Z.B.; Lei, C.K.; Hao, J.C. Damage characteristics of coal microstructure with liquid CO_2 freezing-thawing. *Fuel* **2019**, 249, 169-177.

(116) Meng, Q.R.; Zhao, Y.S.; Kang, Z.Q.; Wang, Y.; Gao, L.; Zhang, Y.F. Evolution of micron-scale pore structure and connectivity of lignite during pyrolysis. *Adv. Mater. Sci. Eng.* **2020**, 9186542.

(117) Feng, Z.J.; Zhao, Y.S. Pyrolytic cracking in coal: Meso-characteristics of pore and fissure evolution observed by micro-CT. *J. China Coal Soc.* **2015**, 40(01), 103-108.

(118) Yu. Y.M.; Liang, W.G.; Hu, Y.Q.; Meng, Q.R. Study of micro-pores development in lean coal with temperature. *Int. J. Rock Mech. Min.* **2012**, 51, 91-96.

(119) Xiao, Y.; Lu, J.H.; Wang, C.P.; Deng, J. Experimental study of high-temperature fracture propagation in anthracite and destruction of mudstone from coalfield using high-resolution microfocus X-ray computed tomography. *Rock Mech. Rock Eng.* **2016**, 49(9), 3723-3734.

(120) Fu, X.L.; Dai, J.S.; Feng, J.W. Prediction of tectonic fractures in coal reservoirs using geomechanical method. *Geosci. J.* **2018**, 22(4), 589-608.

(121) Ju, Y.; Xi, C.D.; Zhang, Y.; Mao, L.T.; Gao, F.; Xie, H.P. Laboratory in situ CT observation of the evolution of 3D fracture networks in coal subjected to confining pressures and axial compressive loads: a novel approach. *Rock Mech. Rock Eng.* **2018**, 51(11), 3361-3375.

(122) Li, Y.Y.; Cui, H.Q.; Zhang, P.; Wang, D.K.; Wei, J.P. Three-dimensional visualization and quantitative characterization of coal fracture dynamic evolution under uniaxial and triaxial compression based on μ-CT scanning. *Fuel* **2020**, 262, 116568.

(123) Yang, Q.; Yu, Y.B.; Cheng, W.M.; Cui, W.T.; Xin, Q.L.; Gao, C.W.; Zheng, L. Porosity and fracture changes of coal under uniaxial strain conditions based on the X-ray microscopic imaging technology. *Energy Fuels* **2021**, 36(1), 320-332.

(124) Wang, D.K.; Tian, X.R.; Wei, J.P.; Zhang, H.T.; Yao, B.H.; Zhang, H.; Chen, C.Y. Fracture evolution and nonlinear seepage characteristic of gas-bearing coal using X-ray computed tomography and the lattice Boltzmann method. *J. Petrol. Sci. Eng.* **2022**, 211, 110114.

(125) Zhang, G.L.; Ranjith, P.G.; Liang, W.G.; Haque, A.; Perera, M.S.A.; Li, D.Y. Stress-dependent fracture porosity and permeability of fractured coal: An in-situ X-ray tomography study. *Int. J. Coal. Geol.* **2019**, 213, 103279.

For Table of Contents Only